Mesospheric temperature estimation from meteor decay times of weak and strong meteor trails

Jeong-Han Kim [a], Yong Ha Kim [b,*], Geonhwa Jee [a], Changsup Lee [b]

[a] Division of Polar Climate Research, Korea Polar Research Institute, 12 Gaetbeol-ro, Yeonsu-gu, Incheon 406-840, Republic of Korea
[b] Department of Astronomy and Space Science, Chungnam National University, 79 Daehangno, Yuseong-gu, Daejeon 305-764, Republic of Korea

ARTICLE INFO

ABSTRACT

Neutral temperatures near the mesopause region were estimated from the decay times of the meteor echoes observed by a VHF meteor radar during a period covering 2007 to 2009 at King Sejong Station (62.22°S, 58.78°W), Antarctica. While some previous studies have used all meteor echoes to determine the slope from a height profile of log inverse decay times for temperature estimation, we have divided meteor echoes into weak and strong groups of underdense meteor trails, depending on the strength of estimated relative electron line densities within meteor trails. We found that the slopes from the strong group are inappropriate for temperature estimation because the decay times of strong meteors are considerably scattered, whereas the slopes from the weak group clearly define the variation of decay times with height. We thus utilize the slopes only from the weak group in the altitude region between 86 km and 96 km to estimate mesospheric temperatures. The meteor estimated temperatures show a typical seasonal variation near the mesopause region and the monthly mean temperatures are in good agreement with SABER temperatures within a mean difference of 4.8 K throughout the year. The meteor temperatures, representing typically the region around the altitude of 91 km, are lower on average by 2.1 K than simultaneously measured SATI OH(6–2) rotational temperatures during winter (March–October).

1. Introduction

A VHF meteor radar has been operated at King Sejong Station (KSS; 62.22°S, 58.78°W), Antarctica since March 2007 for observations of the neutral winds in the mesosphere and lower thermosphere (MLT) region. These radar observations also allow us to estimate the neutral temperature near the mesopause region from the measured decay times of the meteor trails. A number of studies have been devoted to determining the atmospheric parameters such as temperature and pressure (in particular, the atmospheric temperature) from their relation with the diffusion coefficient for the decay of meteor trails, which can be calculated from the measurements of meteor decay times under the assumption of ambipolar diffusion of the ions and electrons within meteor trails (Chilson et al., 1996; Hocking et al., 1997, 2004; Hocking, 1999; Cervera and Reid, 2000; Nielsen et al., 2001; Holdsworth et al., 2006; Kumar, 2007).

However, the diffusion theory and the measurement of meteor decay times can only allow one to compute $T/P^{1/2}$ (T and P are atmosphere temperature and pressure) and thus accurate temperature estimation requires the pre-knowledge of the pressure

and vice versa, which is not normally available. In order to overcome this limitation, Hocking (1999) proposed a new method for the estimation of atmospheric temperature without requiring a knowledge of pressure. Instead of using the direct relationship between the ambipolar diffusion coefficient and the temperature with a known, but often unavailable, pressure, they utilized a least-squares fitting of a first-order polynomial to the logarithmic diffusion coefficient as a function of height and then applied a scale height analysis to determine the temperature (Hocking, 1999; Hocking et al., 2004). According to their method, the atmospheric temperature is assumed to vary with a first-order polynomial near the meteor height at which most meteors are evaporated. Using the first-order polynomial has a limitation to determine only an average temperature in the range of the meteor heights and also requires a mean temperature gradient at the height. However, it has been reported in a number of studies that the mesospheric temperatures estimated from this method are relatively consistent with other ground-based temperature measurements (Singer et al., 2003, 2004; Hocking et al., 2004, 2007; Holdsworth et al., 2006; Stober et al., 2008). For details on the advantage and limitation of this method refer to Hocking et al. (2004).

According to the diffusion theory, the decay time of a meteor trail is inversely proportional to the diffusion coefficient and therefore is a function of atmospheric temperature and pressure.

However it was found that the meteor decay time is also affected by the magnitude of plasma density within meteor trails in addition to the background atmospheric parameters (Ballinger et al., 2008; Singer et al., 2008; Younger et al., 2008; Kim et al., 2010). Kim et al. (2010) further implied that the temperature estimation from the measurements of meteor decay times can be affected by the level of plasma density within meteor trails. Dissipation of meteor trails at low altitudes is largely controlled by diffusion and chemical recombination. At higher altitudes, diffusion dominates the dissipation and the decay time increases with decreasing height. Kim et al. (2010) studied the variations of meteor decay times with height for weak and strong meteors separately and found that the variations of decay time with height are significantly smaller for strong meteors than for weak meteors. Here the weak and strong meteors indicate the low and high plasma densities within meteor trails, respectively. The trail plasma density can be deduced from the strength of radar signal reflected from the trails and the travel distance of the signals. Their study also suggested that only weak meteors should be used for estimating the mesospheric temperature from meteor decay times since the decay of strong meteor trails is controlled not only by diffusion processes but also by chemical recombination processes due to the higher plasma density within strong meteor trails while the decay of weak meteor trails is largely controlled by diffusion process alone.

In this study, we will further investigate the dependency of the temperature estimation on the trail plasma density by applying the method from Hocking (1999) and will also compare the estimated temperatures with other simultaneous measurements from a spectral airglow temperature imager (SATI) and TIMED/SABER instrument.

2. Instruments and data

2.1. The VHF meteor radar

Since the installation in March 2007 at KSS, the meteor radar has been continually observing the mesosphere and lower thermosphere (MLT) region. The radar supplied by ATRAD is an interferometric radar which consists of a cross folded dipole transmitting antenna and 5 receiving antennas arranged along two perpendicular directions with spacings of 2 λ and 2.5 λ to minimize mutual antenna coupling. This follows the design presented by Hocking et al. (1997) and Jones et al. (1998). It operates at 33.2 MHz with a peak power of 8 kW to receive meteor echoes reflected from the underdense meteor trails. This instrument is continuously observing the altitude region of about 70 km to 110 km for 24 h a day, regardless of weather conditions at the site, in contrast to ground-based optical instruments such as spectral airglow temperature imagers (SATI), all-sky cameras (ASC), Michelson interferometers, and Fabry-Perot interferometers (FPI), which are extensively utilized for the observations of the upper atmosphere but only work during clear moonless nighttime. A radio signal transmitted from the transmitting antenna is reflected by a meteor plasma trail and the returning signal is received simultaneously by 5 receiving antennas with a range resolution of 2 km. Interferometric analysis of the received echo signals allows one to determine the location of meteors in the sky and an angular resolution has been generally known to be less than 2°. The configuration of antenna array and information on the VHF meteor radar system with data analysis are described in detail by Jones et al. (1998) and Holdsworth et al. (2004, 2008) including the criteria applied for determining whether the backscattered signal is reflected by the underdense meteor ionized trail or not.

Table 1
Numbers of days in each month for radar operation at King Sejong Station.

	Jan	Feb	Mar	Apr	May	Jun	Jul	Aug	Sep	Oct	Nov	Dec
2007			29	30	31	3	–	–	–	–	24	29
2008	9	–	–	–	6	5	12	31	29	28	26	17
2009	17	28	29	28	19	30	28	30	29	27	3	–

In this study, we analyzed the data observed for the period of March 2007 through November 2009 excluding periods of maintenance breaks. Table 1 shows the numbers of days in each month for radar operation during this period. The number of meteor echoes is about 12,000 to 28,000 per day, which is large enough to apply our data-selection criteria for this study. The all-sky interferometeric meteor radar collects meteor echoes over the full range of zenith angle, but the data used in this study were restricted to the range of zenith angle between 10° and 70° in order to remove unnecessary uncertainties in the data. Meteor echoes with large zenith angles are reflected from near the horizon and may contain significant atmospheric effects due to, for example, water vapor and ions and electrons along the passage of signal, which may cause errors for the determination of the range. The echoes with small zenith angles, on the other hand, are reflected from near the zenithal direction, thereby having small radial velocities, which may cause large errors for the determination of horizontal wind. To ensure unambiguous detections of meteors we limit the data to signal-to-noise ratios better than 7.4 dB. For the comparisons with other simultaneous temperature observations, we additionally restricted the data to the nighttime periods from 1600LT to 0800LT on the next day for winter seasons from March to October and from 1800LT to 0600LT on the next day for summer seasons of November, December, January and February to best enable comparisons with the SATI and SABER temperatures, respectively.

2.2. SATI temperature measurements

A Spectral Airglow Temperature Imager (SATI) has been operated at KSS to measure OH(6–2) and O_2(0–1) airglow emissions by using narrow-band Fabry-Perot interference filters since its installation in 2002 (Chung et al., 2006). It has been known that the peak heights of OH and O_2 emissions are 87 ± 3 km and 95 ± 2 km, respectively (Greer et al., 1986; Baker and Stair, 1988; Yee et al., 1997). The SATI is comprised of a conical mirror, Fresnel lens, interference filter, detector lens, and CCD. The conical mirror gathers light from an annular sky area of radius 29° centered on the zenith, with inner and outer radius of 47 km and 63 km for O_2 altitude, and 43 km and 58 km for OH altitude. Details for the determination of emission rates and rotational temperatures from OH and O_2 airglow measurements are described in Wiens et al. (1997) and Sargoytchev et al. (2004). The SATI at KSS normally operates from March to October, which is winter in Antarctica, except the period near the full moon. For the comparison with estimated meteor temperatures, the SATI temperature measurements were available only for one winter season in 2007 since the instrument had failed to work for the winter periods in 2008 and 2009.

2.3. TIMED/SABER temperature measurements

The Sounding of the atmosphere using broadband emission radiometry (SABER) experiment was onboard the thermosphere ionosphere mesosphere energetics and dynamics (TIMED) satellite to measure the limb radiance in the ten broadband infrared channels ranging from 1.27 μm to 17 μm. From the limb measurement of

CO_2 15 μm channels, the SABER instrument provides the kinetic temperature profile of the atmospheric region extending from 15 km to 120 km altitude. The details of the SABER instrument including the retrieval algorithm of kinetic temperature (T_k) were fully discussed by Mertens et al. (2001, 2002) and only a brief introduction is described here.

The latitudinal coverage of the SABER instrument is governed by a yaw cycle with a period of about 60 day, which allows the observations in the latitudinal range from 83°S to 52°N in the South viewing phase and from 53°S to 82°N in the North viewing phase, because the TIMED satellite orbit precesses by about 3° per day and the SABER instrument must keep its detectors from looking directly at the Sun. For comparison with the meteor temperatures, the SABER temperatures (ver. 1.07) were selected for the locations within ±5° in latitude and longitude around the location of KSS (62.22°S, 58.78°W). For the comparison with the temperatures estimated from meteor decay times, the daily mean temperature profiles were computed during the period of 2007 to 2009 and then the temperature profiles were averaged for the altitude range of 86 km to 96 km as a mean temperature.

3. Meteor decay times

To investigate the dependency of the estimated temperature on the plasma density of meteor trails, we divided the selected data into two groups of meteors, namely weak and strong meteors, according to the estimated relative electron line density along the meteor trail. It has been known that the electron line density along the meteor trail is proportional to (received power × range³)$^{0.5}$ of an observed meteor echo (Singer et al., 2008; Kim et al., 2010). Here, the weak and strong meteors were defined by the lower and upper quartiles of the electron line densities, respectively. The words, "strong" and "weak" should not be interpreted as "overdense" and "underdense", because all the data are from underdense meteors selected by radar detection criteria (Holdsworth et al., 2004). Note that meteor echoes in the weak group mostly travel of the shorter distance from meteor trails to receivers and thus suffer from less range errors. Refer to Kim et al. (2010) for the details of the classification of meteors with the estimated relative electron line density.

The ambipolar diffusion theory predicts that the meteor decay time increases with decreasing altitude due to the enhanced collisions with increasing neutrals. However, recent meteor radar observations reported that the decay time becomes smaller at lower altitudes below about 80–85 km, especially at high latitude regions (Hall et al., 2005; Ballinger et al., 2008; Singer et al., 2008; Younger et al., 2008). Fig. 1 shows the altitude profiles of monthly decay times taken from the VHF meteor radar at KSS during southern summer (Dec. 2007) and winter (Jun. 2008). It is clear that as the altitude decreases the increasing decay times turn to decreasing values at about 85 km in summer and about 80 km in winter. This change of decay times has been discussed in earlier studies (Ballinger et al., 2008; Singer et al., 2008; Younger et al., 2008), which suggested that there should be additional removal processes of meteor trail plasma such as the ice and dust particle effects and ion-electron recombination process etc. Kim et al. (2010) further showed that the observed height profiles can be explained quantitatively by a simple model including the ambipolar diffusion and the empirical electron recombination obtained from rocket experiments. Fig. 1 also shows that the decay times deviate from the diffusion-dominated behavior at above about 95 km altitude. This behavior was explained by the effects of the geomagnetic field on the trail plasma motion due to the reduced collision frequency with neutrals at higher altitude (Jones, 1991; Dyrud et al., 2001; Hocking, 2004a). The behaviors of meteor decay times at these lower and higher altitudes indicate that the ambipolar diffusion can be applied only to the relatively narrow altitude region of ∼85 km to ∼95 km. This also implies that only the decay times within this altitude region should be utilized to estimate the temperature (Kim et al., 2010). In this study, therefore, we restricted the altitudes of meteor data to the range of 86 to 96 km for the temperature estimation. Most of previous studies used the lower limit of the altitude below 86 km (Cervera and Reid, 2000; Hocking 2004a; Holdsworth et al., 2006; Stober et al., 2008). However, our meteor data show the decreasing tendency of decay times at lower altitudes due to electron recombination in addition to diffusion, as explained in Kim et al. (2010).

As for the zenith angle of the incoming meteors, an example of zenith angle distributions is shown in Fig. 2 for the weak and strong meteors on March 3, 2007. As discussed in Kim et al. (2010), the weak and strong meteor groups are strongly dependent on the distance range that meteor echoes travel from meteor trails to receivers. Fig. 2 implies that the weak meteors travel over the relatively small ranges from the meteor trails to the receivers along the path with relatively small zenith angles since their
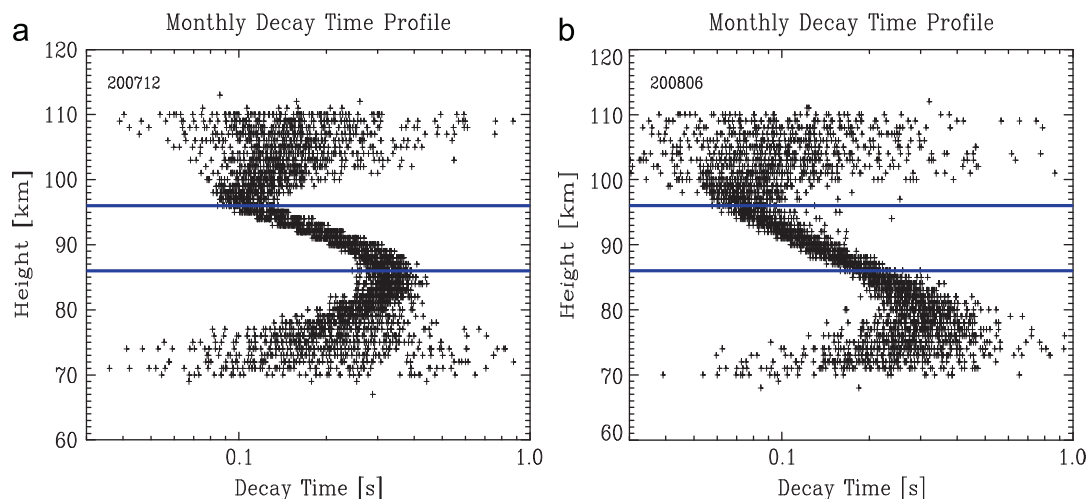
Fig. 1. Monthly decay time profiles during southern summer (a) and winter (b). Each data point (cross) indicates 15 min averaged decay time and the height range between 86 km and 96 km is marked with blue solid lines (see text). (For interpretation of the references to color in this figure legend, the reader is referred to the web version of this article.)
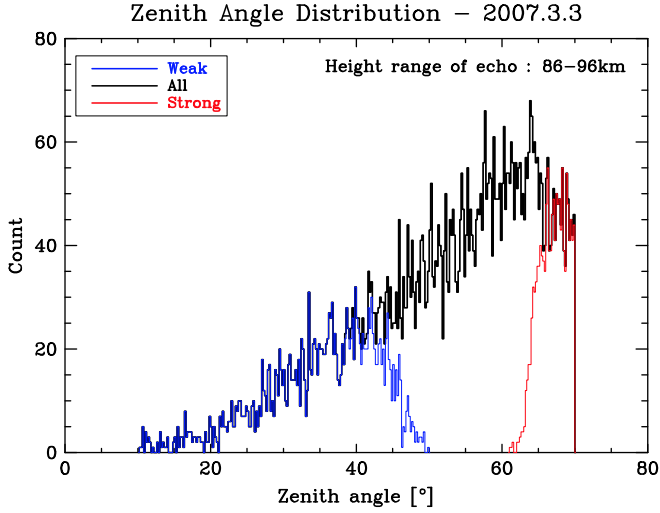
Fig. 2. Zenith angle distributions of meteor echoes on March 3, 2007 in the altitude range of 86–96 km. Note that meteors in the weak and strong groups are concentrated with zenith angle less than 50° and greater than 60°, respectively.

echoes are weak due to the lower plasma density and thus the echoes only traveling over the short distance can be detected above the receiver's limit. On the other hand, the echoes from the strong meteors can maintain their signals to reach the receiver antenna over a long range at large zenith angles.

4. Temperature estimation from meteor decay times

If the ambipolar diffusion is the only process of the decay of a underdense meteor, the diffusion coefficient and decay time have a following relationship (McDaniel and Mason, 1973; Jones and Jones, 1990; Hocking et al., 1997; Hocking, 1999);

$$D_a = \frac{\lambda^2 \ln 2}{16\pi^2 \tau_{1/2}} \qquad (1)$$

where λ is a radar transmitting wavelength, and $\tau_{1/2}$ is a meteor decay time defined as the time that the amplitude of reflected signal falls to one-half of its maximum amplitude. The diffusion coefficient, D_a, is known to depend on atmospheric temperature and pressure as

$$D_a \approx C \frac{T^2}{P} \qquad (2)$$

where T and P are the atmospheric temperature and pressure, and C is a constant including the zero field mobility factor (e.g., Cervera and Reid, 2000). As can be seen from Eqs. (1) and (2), the temperature estimation from meteor decay times or diffusion coefficients is possible only when the information of atmospheric pressure is available. However, the atmospheric pressure near the meteor height is highly variable with altitude and its measurements are not accurate enough to be used for the study of temperature estimation. Hocking (1999) then proposed a new method of estimating temperature to overcome this limitation. It assumes, instead of an isothermal atmosphere, a linearly varying atmospheric temperature with altitude as

$$T = T_0 + T_g z' \qquad (3)$$

where T_0 and $T_g = dT/dz$ are the temperature and the vertical temperature gradient at $z' = 0$ (i.e., meteor peak height), respectively (Hocking, 1999; Singer et al., 2004). Recognizing the relationship between the meteor decay time and the diffusion coefficient that is the function of the atmospheric temperature

and pressure as in Eq. (2), with the atmospheric pressure profile, $P = P_0 \exp\{-\int(mg/kT)dz\}$, one can estimate a mean temperature at meteor peak height from the slope, S, of the scatter plot of $\log_{10}(1/\tau_{1/2})$ vs. height and the temperature gradient T_g as

$$T_0 = S\left(2T_g + \frac{mg}{k}\right)\log_{10} e \qquad (4)$$

where k is Boltzmann constant, g is the gravitational constant at meteor peak height, and m is the mass of typical atmosphere molecules. According to this expression for the mean temperature, the slope and temperature gradient need to be determined.

The slope S can be determined from the linear relationship between $\log_{10}(1/\tau_{1/2})$ and height. Before determining the slope from the scatter plot, it might be necessary to remove unrepresentative data such as outliers in the scatter plot in order to improve the accuracy of determined slopes (Hocking et al., 1997; Cervera and Reid, 2000). However, we do not apply this procedure to our data since each study applied different criteria for defining the outliers and there is no definitive way of selecting and removing the outliers. Furthermore, any changes of the slope in Eq. (4), for instance, by removing outliers can directly affect the resulting temperature. Therefore the removal process may not guarantee the improvement of the accuracy of the resulting temperature. Most recently, Holdsworth et al. (2006) utilized the Statistical Comparison Technique (SCT) originally developed by Hocking et al. (2001) to determine the slope with a correction factor to consider the errors in both measurements of height and decay time. Once the optimum data sample for the logarithmic inverse decay time $d = \log_{10}(1/\tau_{1/2})$ versus height h is selected for temperature estimation, one can determine the slope S_d or S_h from the least square fitting by taking d or h as an independent variable, respectively. Most of previous studies have used S_d for their temperature estimation (e.g., Holdsworth et al., 2006) but we will try both d and h as an independent variable and find the appropriate slope for our data set before applying the SCT correction factor.

The secondary factor needed in Eq. (4) is the temperature gradient T_g, in principle, at the meteor peak height, where determination of the slope is most weighted. Although the meteor peak height varies within altitudes of 89–92 km over the season, our criterion for the meteor sample is fixed to be in the altitude range of 86–96 km, and thus temperature estimation from Eq. (4) effectively needs an average temperature gradient in this altitude range. Since the mesopause is usually located within this altitude range during all seasons, the average temperature gradient is expected to be small. From a number of studies using model simulations and observational data from rocket, ground-based and satellite measurements, it is generally known that the mesopause altitude is lowest in summer but highest in winter (Lübken and Von Zahn, 1991; Lübken, 1999; Friedman and Chu, 2007; Xu et al., 2007). Therefore the average temperature gradient (over 86–96 km) tends to be positive in summer when the mesopause is typically located below the middle altitude of the sampling heights (91 km), but it is expected to be negative in winter when the mesopause altitude is higher than 91 km. However, the relative altitudes of the mesopause and meteor peak region can also significantly vary with local time, affecting the average temperature gradient further. Several techniques have been devised for the estimation of local temperature gradient at the meteor peak height by using empirical models or data from satellite and ground-based observations (Hocking et al., 2004; Singer et al., 2004; Holdsworth et al., 2006; Stober et al., 2008).

In this study, we developed a temperature gradient model for our meteor sample by averaging the temperatures of TIMED/SABER between 86 km and 96 km height in the daily temperature

profile during 2003 through 2009 over the location of KSS. However, since the satellite observation has missing periods over the location of KSS due to the SABER yaw cycle, it was supplemented by the temperature gradient model presented by Holdsworth et al. (2006) for Davis Station, Antarctica (68.6°S, 78.0°E) which is located at similar latitude to KSS (62.22°S, 58.78°W). The temperature gradient model considering annual, semiannual, and terannual components is shown in Fig. 3 with SABER (triangles) and Davis (crosses) temperature gradients. It should be noted that Davis temperature gradient model was developed using OH temperatures with the representative altitude of about 87 km while our temperature gradient model represent the altitude of 91 km. Furthermore, the two stations are located at very different longitude sectors, contributing to discrepancy between two temperature gradient models. However, the variation of our temperature gradient model is within 1 K/km from Davis model throughout a year and can be considered to be comparable with the SABER temperature gradients. Difference of 1 K/km in temperature gradient produces on average only about 10 K difference in the temperature estimation.

5. Results and discussions

5.1. Slope S

Temperature estimation from meteor decay times in Eq. (4) requires the slope of the least-squares best fit line from the scatter plot of the logarithmic inverse decay time d versus height h. Examples of the scatter plots are shown in Fig. 4 for the nighttime (1800LT–0600LT) data on March 03, 2007. As indicated in Fig. 1, the decay times were selected within the 86 km to 96 km altitude region in which the ambipolar diffusion dominates the plasma diffusion of meteor trails. The selected decay time data were divided into the weak and strong underdense meteor groups according to the plasma line density of meteor trails, which are presented in Fig. 4(a) and (b), respectively. For each meteor group the estimated slopes are displayed with green, blue, and red lines for different ways of determining the slopes. Considering the definition of the line density, the meteor echoes from the weak meteor trails tend to reach the receiver at a relatively small zenith angle but the echoes from the strong meteor trails tend to travel
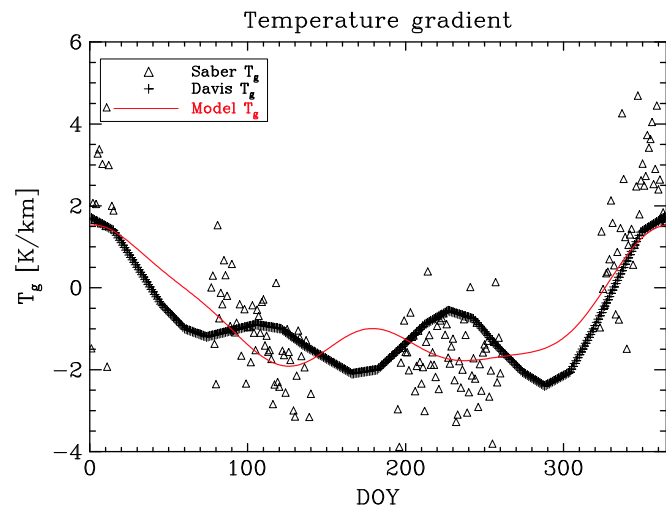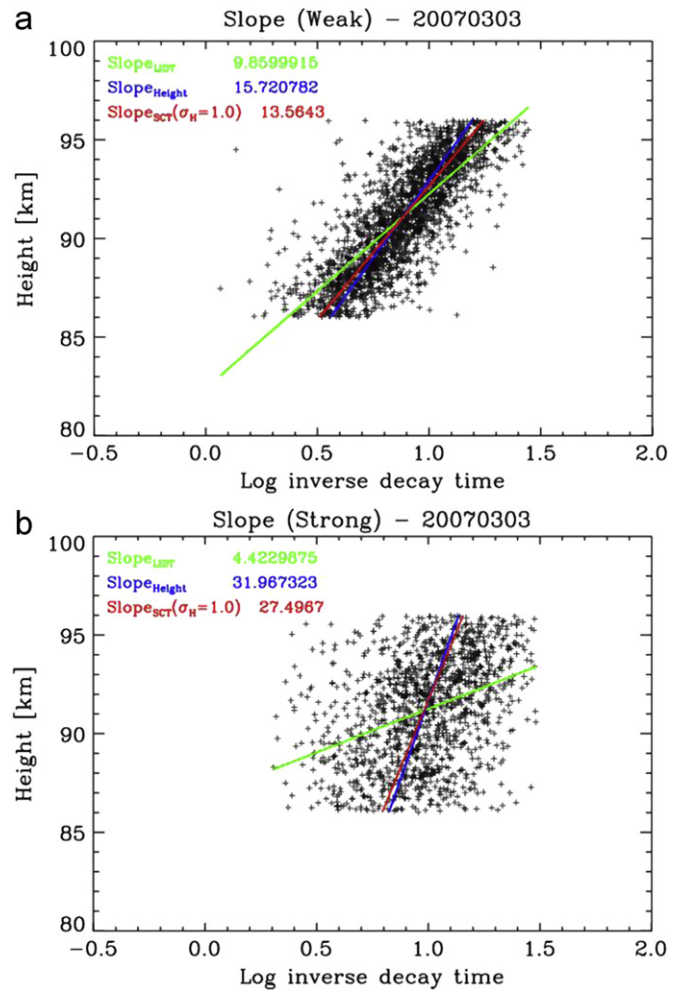
Fig. 4. Scatterplots of LIDT as a function of height for the weak and strong meteor groups measured on March 3, 2007. Upper and lower panels show slope determination for the weak and strong groups, respectively. The solid lines of green, blue, and red colors indicate linear fits using d and h as the independent variables, and linear fit using SCT method for height with σ_h of 1.0, respectively. (For interpretation of the references to color in this figure legend, the reader is reffered to the web version of this article.)

at a large zenith angle as in Fig. 2. Holdsworth et al. (2006) limited their slope estimation to meteor echoes with zenith angles below 60° since their estimation showed that the inclusion of echoes with zenith angles beyond 60° reduce the estimated temperature by about 8%. Note that their limitation of zenith angle turns out to be almost equivalent to excluding the meteor echoes from the strong meteor trails in our study; that is, by limiting the zenith angle to below 60° they were selecting the meteor echoes mostly from the weak meteor group but without recognizing the small plasma line density of the selected meteor trails.

Previous studies mostly chose the logarithmic inverse decay time d as an independent variable in their determination of the slope because the observational error of decay time is generally smaller than the error of measured height and directly applied on temperature estimation (e.g., Hocking, 1999; Hocking et al., 2001; Stober et al., 2008). In this study, we initially tried to determine the slope using both d and h as independent variables on the least square fit. However, we found that in our data set the h-independent slope is more appropriate than the d-independent slope. The slopes of the scatter plot in Fig. 4 were determined by least-squares fitting with two independent variables d and h, which were displayed with green and blue lines, respectively. It seems to be intuitively very clear that the estimated slopes S_d

Fig. 3. Model of the vertical temperature gradient (red) around 91 km for the location of King Sejong Station (62°S, 59°W). The model is the result of harmonic fit with annual, semiannual, and terannual components using daily mean SABER temperature gradient at 91 km (triangles) and Holdsworth et al. (2006)'s temperature gradient model (crosses).

with the independent variable d (green lines) do not represent the actual slope of the scatter plots for both the weak and strong groups. This is because the meteor sample was selected within 86–96 km, but no decay time was excluded. On the other hand, the slopes S_h with the independent variable h (blue lines) seem to reasonably well represent the behavior of decay time with height. Therefore, we have chosen the latter slope S_h and applied the following SCT correction factor to the slope as displayed with red lines in Fig. 4:

$$S_{SCT} = \left(1 - \left(\frac{\varepsilon_h}{\sigma_h}\right)^2\right) S_h \qquad (5)$$

where ε_h is the measurement error in h and σ_h is the standard deviation of the height determined from the measured range and zenith angle (Hocking et al., 2001). The standard deviation σ_h of the vertical meteor height can easily be determined from the radar measurements of range and zenith angle for meteor echoes. Although the measurement error ε_h may vary with the specification and performance of each radar system, Hocking (2004b) estimated this error to be about 3 km from the result of numerical model study for a pulse length equivalent to 2 km, and a meteor at an altitude of 90 km at an angle of 50° from zenith. We computed the SCT slope using the measurement error ε_h as a free parameter and found that the estimated temperature from the weak group with ε_h of 1.0 km is in good agreement with the temperature from other measurements. This value of 1.0 km is consistent with the result of Holdsworth et al. (2006), which assumed the observational height error equivalent to about 1.1 km.

As can be seen in Fig. 4, it is clear that there is a narrow band in the height profile of the weak meteor group and the SCT slope (red line) represents the variation of d with height reasonably well. On the other hand, in the height profile of the strong group the distribution of meteor decay times is considerably scattered and does not show the clear stream in d with respect to h, height. The slope from the strong group is defined poorly and thus it may not properly represent the variation of d with height, leading to unreliable temperature estimation. This is consistent with the result by Kim et al. (2010), which shows that the height profiles of monthly mean decay times from the strong meteor group do not obey the decay time height profile of ambipolar diffusion assumption whereas those from the weak meteor group show clear agreement with the decay time height profile of ambipolar diffusion assumption.

The seasonal variation of the slopes determined from the weak meteor group shows a minimum during southern summer and a maximum during winter, which is similar to the temperature variation with season at southern hemisphere, because the slope plays a more important role on temperature estimation than the temperature gradient. This seasonal variation in the determined slopes is consistent with the results of Hocking (1999). The variation of the slopes with seasons may be small at most of mid- and low-latitude regions, but it can be crucial at high latitude regions because of the large mean temperature variation between summer and winter near meteor maximum altitude (Hocking, 1999). In this study, we thus utilize the temperature estimated from the weak meteor group only using the SCT slope, referred to simply as the "meteor temperature" in later discussion.

5.2. Temperature estimation

Fig. 5(a) shows the daily meteor temperatures during a period from March 2007 to November 2009. The monthly SABER temperatures during 2007 through 2009 and, SATI OH and O₂ rotational
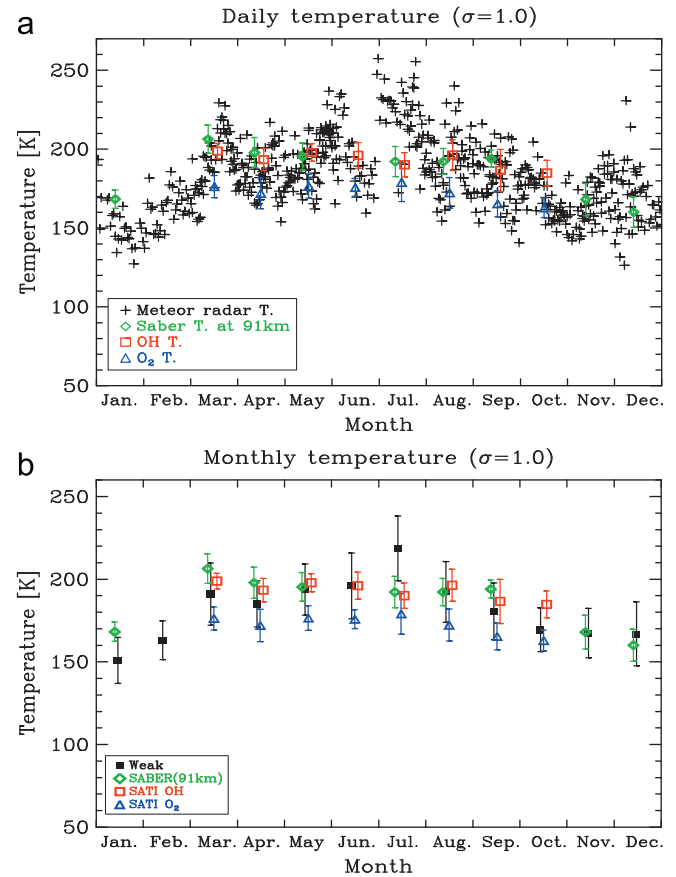
Fig. 5. Daily (a) and monthly mean (b) temperatures estimated from decay times of the weak meteor group using the temperature gradient model and height-independent slope applying σ_h of 1.0 km. The SABER temperatures around 91 km, and SATI OH and O₂ rotational temperatures are superimposed with the colors of green, red, and blue, respectively. (For interpretation of the references to color in this figure legend, the reader is reffered to the web version of this article.)

temperatures during 2007 are superimposed with the symbols of diamond, square, and triangle, respectively. As mentioned previously, because the slope has more impact on temperature estimation than temperature gradient, the seasonal variation of the estimated temperatures shows a similar trend to that of the determined slope.

The seasonal variation of the meteor temperatures is consistent with the results of other studies, which investigated the mesospheric temperature estimation from meteor decay times at various sites in the northern and southern hemispheres (Singer et al., 2003, 2004; Hocking et al., 2004; Holdsworth et al., 2006; Stober et al., 2008). In general, the annual variation of mesospheric temperatures, which show a minimum during southern summer and maximum during winter, may be explained by the large-scale circulation in which air is transported from the summer pole to the winter pole, resulting in adiabatic cooling and heating at the summer and winter poles, respectively (Garcia and Solomon, 1985).

The variations of meteor temperatures between summer and winter are typically less than about 30 K at northern middle latitudes (Hocking, 1999; Stober et al., 2008) and greater than 40 K at northern and southern high latitudes (Singer et al., 2003, 2004; Hocking et al., 2004; Holdsworth et al., 2006), implying relatively large variation of mesospheric temperature at high latitude regions. From our results, the summer to winter variation of meteor temperatures is around 40–50 K, which is comparable with the results of other studies.

We compared the meteor temperatures with SATI OH and O_2 temperatures day by day, while previous studies (Hocking et al., 2004, 2007; Holdsworth et al., 2006) compared mean temperatures estimated from meteors over 2–7 day with those of other measurements. For the 54 simultaneously observed days in 2007, the correlations between our daily mean meteor temperatures and, SATI OH and O_2 rotational temperatures are 0.1 and 0.26, respectively. These low correlations between the meteor and SATI rotational temperatures seem to imply that SATI temperatures are representing only narrow airglow layers (possibly also varying in height over time), whereas the meteor temperatures are reflecting a wide range (10 km in our analysis) of altitude around the meteor peak altitude. We will investigate further the relation between the meteor and SATI temperatures with more number of simultaneously observed data in the future.

5.3. Comparison of monthly mean temperatures

In order to compare the differences among the temperatures inferred from the meteors, SABER and SATI instruments without regard to daily variation, we computed the monthly mean meteor temperatures as shown in Fig. 5(b). The absolute values of the meteor temperatures during fall through spring are slightly smaller than those of Holdsworth et al. (2006), while they are in a good agreement with the SABER mean temperature near 91 km that was averaged over the altitudes of 86–96 km using the SABER data during 2007 through 2009. The monthly mean meteor temperature variation is generally consistent with OH(6–2) and $O_2(0–1)$ rotational temperatures from SATI measurements over KSS. The mean meteor temperature from March through October is lower by 2.1 K and higher by 18.3 K than the mean OH and O_2 rotational temperatures, respectively.

Although the variations of mesopause height with the location and season are not clear yet, it has been generally known that the mesopause altitude is higher than 95 km in winter and lower than 90 km in summer (She and Lowe, 1998; Kawahara et al., 2002; Xu et al., 2007). During winter, the meteor temperatures representing the atmospheric temperature around 91 km generally exist between the rotational temperatures of OH and O_2 emissions, whose layers are known to be at the altitudes of about 87 ± 3 km and 95 ± 2 km, respectively (Baker and Stair, 1988; Yee et al., 1997).

The meteor temperatures seem to be generally consistent with the SABER monthly mean temperatures, although slightly lower. Differences are largest in January, when the largest discrepancies reach about 20 K. This difference during southern summer may be due to the sparse SABER data during January and February over the location of KSS, and the relatively large uncertainty of SABER temperature in the high-latitude MLT region.

Recently, many studies have been dedicated to evaluating SABER temperature extensively by comparison with the temperatures from various instruments such as SATI, lidar, spectrometer, in-situ measurement, and AURA/MLS and also by validating the temperature retrieval algorithms from CO_2 15 μm radiance measurements considering non-LTE effects (Mertens et al., 2004; Kutepov et al., 2006; Lpez-González et al., 2007; García-Comas et al., 2008; Remsberg et al., 2008; Smith et al., 2010; French and Mulligan, 2010). García-Comas et al. (2008) reported that the error of SABER temperature with non-LTE model parameters near 90 km is around ± 8 K for polar summer and less than ± 2 K for other seasons. Remsberg et al. (2008) studied the error of SABER temperature (v1.07) by comparison with the temperatures measured from airglow, Na lidar, and falling sphere experiment, and reported the estimates of a systematic error (1.3 K at 80 km, 3.6 K at 90 km, and 1.4 K at 100 km) and a noise error (2.7 K at 80 km, 8.9 K at 90 km and 8.9 K at 100 km) for polar summer. García-

Comas et al. (2008) presented that the error of SABER temperature caused by non-LTE model parameters near 90 km are around ± 8 K for polar summer and less than ± 2 K for other season. In addition, Remsberg et al. (2008) showed that the July average temperatures of the SABER (v1.07) profiles obtained from its profiles at $69 \pm 5°$N and at $16 \pm 20°$E during 2002 through 2007 are higher than the falling sphere climatology by about 10 K, 20 K, and 15 K for the altitudes of 87 km, 90 km, and 92 km, respectively. They also stated that the mesopause altitude from the SABER temperature profile in July is lower than that of the falling sphere climatology by 1.5 km. The result of Remsberg et al. (2008) on the mesopause altitude is consistent with the result of Kutepov et al. (2006) who reported that the mesopause altitude in SABER profile is lower than that of climatological and falling sphere data by 2 km even after accounting for the CO_2 ν_2 quanta V–V exchange. Our temperatures deduced from meteor decay times during the entire period are lower on average by 4.8 K than the SABER temperatures, which may be reasonable, given the systematic errors of the SABER temperatures.

While the mesospheric temperature in the high latitude region has been investigated by many studies, it is still difficult to understand the local trend and characteristics owing to observational limitations, especially in the southern hemisphere. This may be one of the most important reasons that many studies have been dedicated to estimating the mesospheric temperature from meteor radar observations because of their ability to operate around the clock throughout the year. Lübken et al. (1999) reported that the mesospheric temperatures from falling sphere measurements at Rothera Station (68°S, 68°W), Antarctica, during January and February 1998 are typically in the range of 130–150 K at the mesopause altitude between approximately 85 km and 90 km, which is lower by about 20 K than the meteor estimated temperatures in this study. Since they presented an RMS deviation of 16 K from the mean temperature around 90 km, their temperatures are not significantly different from our temperatures that were deduced from the meteors in the altitude range of 86–96 km.

6. Summary and conclusions

In this study, we have analyzed VHF meteor radar data obtained at King Sejong Station (62.22°S, 58.78°W) during a period from March 2007 to November 2009 to estimate mesospheric temperatures. The resulting temperatures have been compared with the other simultaneous temperature measurements from SATI for the period from March through October 2007 and from TIMED/SABER for the period from 2007 through 2009.

For temperature estimation from the meteor decay times, we divided the observed (underdense) meteor echoes into weak and strong groups, according to the estimated relative electron line density along meteor trails, and restricted to the height range between 86 km and 96 km where ambipolar diffusion is dominant in the decay process of meteor trails. The height profiles of meteor decay time from the strong group show considerably scattered distributions with height, whereas those from the weak group are relatively well defined. For temperature estimation, therefore, we utilized the decay times only from the weak meteor group and applied Hocking (1999)'s method with SCT correction. The annual variation of the estimated temperatures shows a minimum during southern summer and is in a good agreement with the results from other sites in both the southern and northern hemispheres. The estimated temperatures during southern fall through spring, which are slightly lower than those for Davis Station presented by Holdsworth et al. (2006), are in good agreement with SABER mean temperatures at 91 km for the

location of King Sejong Station, and are also comparable with the SATI OH and O_2 rotational temperatures that were simultaneously measured at the location.

References

Baker, D.J., Stair Jr., A.T., 1988. Rocket measurements of the altitude distributions of the hydroxyl airglow. Physica Scripta 37, 611–622.
Ballinger, A.P., Chilson, P.B., Palmer, R.D., Mitchell, N.J., 2008. On the validity of the ambipolar diffusion assumption in the polar mesopause region. Annales Geophysicae 26 (11), 3439–3443.
Cervera, M.A., Reid, I.M., 2000. Comparison of atmospheric parameters derived from meteor observations with CIRA. Radio Science 35 (3), 833–843.
Chilson, P.B., Czechowsky, P., Schmidt, G., 1996. A comparison of ambipolar diffusion coefficients in meteor trains using VHF radar and UV lidar. Geophysical Research Letters 23 (20), 2745–2748.
Chung, J.-K., Kim, Y.H., Won, Y.-I., Moon, B.K., Oh, T.H., 2006. Observation of temperatures and emission rates from the OH and O_2 nightglow over a southern high latitude station. Advances in Space Research 38 (11), 2374–2379.
Dyrud, L.P., Oppenheim, M.M., vom Endt, A.F., 2001. The anomalous diffusion of meteor trails. Geophysical Research Letters 28 (14), 2775–2778.
French, W.J.R., Mulligan, F.J., 2010. Stability of temperatures from TIMED/SABER v1.07 (2002–2009) and Aura/MLS v2.2 (2004–2009) compared with OH(6–2) temperatures observed at Davis Station, Antarctica. Atmospheric Chemistry and Physics 10, 11439–11446.
Friedman, J.S., Chu, X., 2007. Nocturnal temperature structure in the mesopause region over the Arecibo observatory (18.35°N, 66.75°W): seasonal variations. Journal of Geophysical Research 112, D14107.
Garcia, R.R., Solomon, S., 1985. The effect of breaking gravity waves on the dynamics and chemical composition of the mesosphere and lower thermosphere. Journal of Geophysical Research 90 (D2), 3850–3868.
García-Comas, M., Lpez-Puertas, M., Marshall, B.T., Wintersteiner, P.P., Funke, B., Bermejo-Pantalen, D., Mertens, C.J., Remsberg, E.E., Gordley, L.L., Mlynczak, M.G., Russell III, J.M., 2008. Errors in sounding of the atmosphere using broadband emission radiometry (SABER) kinetic temperature caused by non-local-thermodynamic-equilibrium model parameters. Journal of Geophysical Research 113, D24106.
Greer, R.G.H., Murtagh, D.P., McDADE, I.C., Dickinson, P.H.G., Thomas, L., Jenkins, D.B., Stegman, J., Llewellyn, E.J., Witt, G., Mackinnon, D.J., williams, E.R., 1986. ETON 1: a database pertinent to the study of energy transfer in the oxygen nightglow. Planetary and Space Science 34 (9), 771–788.
Hall, C.M., Aso, T., Tsutsumi, M., Nozawa, S., Manson, A.H., Meek, C.E., 2005. Testing the hypothesis of the influence of neutral turbulence on the deduction of ambipolar diffusivities from meteor trail expansion. Annales Geophysicae 23 (3), 1071–1073.
Hocking, W.K., Thayaparan, T., Jones, J., 1997. Meteor decay times and their use in determining a diagnostic mesospheric temperature-pressure parameter: methodology and one year of data. Geophysical Research Letters 24 (23), 2977–2980.
Hocking, W.K., 1999. Temperatures using radar-meteor decay times. Geophysical Research Letters 26 (21), 3297–3300.
Hocking, W.K., Thayaparan, T., Franke, S.J., 2001. Method for statistical comparison of geophysical data by multiple instruments which have differing accuracies. Advances in Space Research 27 (6–7), 1089–1098.
Hocking, W.K., 2004a. Experimental radar studies of anisotropic diffusion of high altitude meteor trails. Earth Moon and Planets 95 (1–4), 671–679.
Hocking, W.K., 2004b. Radar meteor decay rate variability and atmospheric consequences. Annales Geophysicae 22, 3805–3814.
Hocking, W.K., Singer, W., Bremer, J., Mitchell, N.J., Batista, P., Clemesha, B., Donner, M., 2004. Meteor radar temperatures at multiple sites derived with SKiYMET radars and compared to OH, rocket and lidar measurements. Journal of Atmospheric and Solar-Terrestrial Physics 66 (6−9), 585–593.
Hocking, W.K., Argall, P.S., Lowe, R.P., Sica, R.J., Ellinor, H., 2007. Height-dependent meteor temperatures and comparisons with lidar and OH measurements. Canadian Journal of Physics 85 (2), 173–187.
Holdsworth, D.A., Reid, I.M., Cervera, M.A., 2004. Buckland Park all-sky interferometric meteor radar. Radio Science 39 (5), RS5009.
Holdsworth, D.A., Morris, R.J., Murphy, D.J., Reid, I.M., Burns, G.B., French, W.J.R., 2006. Antarctic mesospheric temperature estimation using the Davis mesosphere–stratosphere–troposphere radar. Journal of Geophysical Research 111, D05108.
Holdsworth, D.A., Murphy, D.J., Reid, I.M., Morris, R.J., 2008. Antarctic meteor observations using the Davis MST and meteor radars. Advances in Space Research 42 (1), 143–154.

Jones, J., Webster, A.R., Hocking, W.K., 1998. An improved interferometer design for use with meteor radars. Radio Science 33 (1), 55–65.
Jones, W., Jones, J., 1990. Ionic diffusion in meteor trains. Journal of Atmospheric and Terrestrial Physics 52 (3), 185–191.
Jones, W., 1991. Theory of diffusion of meteor trains in the geomagnetic field. Planetary Space Science 39 (9), 1283–1288.
Kawahara, T.D., Kitahara, T., Kobayashi, F., Saito, Y., Nomura, A., She, C.-Y., Krueger, D.A., Tsutsumi, M., 2002. Wintertime mesopause temperatures observed by lidar measurements over Syowa station (69°S, 39°E), Antarctica. Geophysical Research Letters 29 (15), 1709.
Kim, J.-H., Kim, Y.H., Lee, C.-S., Jee, G., 2010. Seasonal variation of meteor decay times observed at King Sejong Station (62.22°S, 58.78°W), Antarctica. Journal of Atmospheric and Solar-Terrestrial Physics 72, 883–889.
Kumar, K.K., 2007. Temperature profiles in the MLT region using radar-meteor trail decay times: Comparison with TIMED/SABER observations. Geophysical Research Letters 34, L16811.
Kutepov, A.A., Feofilov, A.G., Marshall, B.T., Gordley, L.L., Pesnell, W.D., Goldberg, R.A., Russel III, J.M., 2006. SABER temperature observations in the summer polar mesosphere and lower thermosphere: Importance of accounting for the CO_2 υ_2 quanta V–V exchange. Geophysical Research Letters 33, L21809.
Lpez-González, M.J., García-Comas, M., Rodríguez, E., Lpez-Puertas, M., Shepherd, M.G., Shepherd, G.G., Sargoytchev, S., Aushev, V.M., Smith, S.M., Mlynczak, M.G., Russell, J.M., Brown, S., Cho, Y.-M., Wiens, R.H., 2007. Ground-based mesospheric temperatures at mid-latitude derived from O_2 and OH airglow SATI data: comparison with SABER measurements. Journal of Atmospheric and Solar-Terrestrial Physics (69), 2379–2390.
Lübken, F.-J., von Zahn, U., 1991. Thermal structure of the mesopause region at polar latitudes. Journal of Geophysical Research 96 (D11), 20841–20857.
Lübken, F.-J., 1999. Thermal structure of the arctic summer mesosphere. Journal of Geophysical Research 104 (D8), 9135–9149.
Lübken, F.-J., Jarvis, M.J., Jones, G.O.L., 1999. First in situ temperature measurements at the Antarctic summer mesopaue. Geophysical Research Letters 26 (24), 3581–3584.
McDaniel, E.W., Mason, E.A., 1973. The Mobility and Diffusion of Ions in Gases. John Wiley and Sons, New York.
Mertens, C.J., Mlynczak, M.G., López-Puertas, M., Wintersteiner, P.P., Picard, R.H., Winick, J.R., Gordley, L.L., Russell III, J.M., 2001. Retrieval of mesospheric and lower thermospheric kinetic temperature from measurements of CO_2 15 μm Earth limb emission under non-LTE conditions. Geophysical Research Letters 28 (7), 1391–1394.
Mertens, C.J., Mlynczak, M.G., López-Puertas, M., Wintersteiner, P.P., Picard, R.H., Winick, J.R., Gordley, L.L., Russell III, J.M., 2002. Retrieval of kinetic temperature and carbon dioxide abundance from non-local thermodynamic equilibrium limb emission measurements made by the SABER experiment on the TIMED satellite. Proceedings of SPIE, Remote Sensing of Clouds and the Atmosphere VII, Agia, Greece, vol. 4882, 162–171.
Mertens, C.J., Schmidlin, F.J., Goldberg, R.A., Remsberg, E.E., Pesnell, W.D., Russell III, J.M., Mlynczak, M.G., López-Puertas, M., Wintersteiner, P.P., Picard, R.H., Winick, J.R., Gordley, L.L., 2004. SABER observations of mesospheric temperatures and comparisons with falling sphere measurements taken during the 2002 summer MaCWAVE campaign. Geophysical Research Letters 31, L03105.
Nielsen, K.P., Röttger, J., Sigernes, F., 2001. Simultaneous measurements of temperature in the upper mesosphere with an Ebert-Fastie spectrometer and a VHF meteor radar on Svalbard (78°N, 16°E). Geophysical Research Letters 28 (5), 943–946.
Remsberg, E.E., Marshall, B.T., Garcia-Comas, M., Krueger, D., Lingenfelser, G.S., Martin-Torres, J., Mlynczak, M.G., Russell III, J.M., Smith, A.K., Zhao, Y., Brown, C., Gordley, L.L., Lopez-Gonzalez, M.J., Lopez-Puertas, M., She, C.-Y., Taylor, M.J., Thompson, R.E., 2008. Assessment of the quality of the Version 1.07 temperature-versus-pressure profiles of the middle atmosphere from TIMED/SABER. Journal of Geophysical Research 113, D17101.
Sargoytchev, S.I., Brown, S., Solheim, B.H., Cho, Y.-M., Shepherd, G.G., Lopez-Gonzalez, M.J., 2004. Spectral airglow temperature imager (SATI): a ground-based instrument for the monitoring of mesosphere temperature. Applied Optics 43 (30), 5712–5721.
She, C.Y., Lowe, R.P., 1998. Seasonal temperature variations in the mesopause region at mid-latitude: comparison of lidar and hydroxyl rotational temperatures using WINDII/UARS OH height profiles. Journal of Atmospheric and Solar-Terrestrial Physics 60, 1573–1583.
Singer, W., Bremer, J., Hocking, W.K., Weiss, J., Latteck, R., Zecha, M., 2003. Temperature and wind tides around the summer mesopause at middle and arctic latitudes. Advances in Space Research 31 (9), 2055–2060.
Singer, W., Bremer, J., Weiß, J., Hocking, W.K., Höffner, J., Donner, M., Espy, P., 2004. Meteor radar observations at middle and Arctic latitudes Part 1: Mean temperatures. Journal of Atmospheric and Solar-Terrestrial Physics 66 (6−9), 607–616.
Singer, W., Latteck, R., Millan, L.F., Mitchell, N.J., Fiedler, J., 2008. Radar backscatter from underdense meteors and diffusion rates. Earth Moon Planet 102, 403–409.
Smith, S.M., Baumgardner, J., Mertens, C.J., Russell, J.M., Mlynczak, M.G., Mendillo, M., 2010. Mesospheric OH temperatures: simultaneous ground-based and SABER OH measurements over Millstone Hill. Advances in Space Research 45, 239–246.

Stober, G., Jacobi, Ch., Fröhlich, K., Oberheide, J., 2008. Meteor radar temperatures over Collm (51.3°N, 13°E). Advances in Space Research 42 (7), 1253–1258.

Wiens, R.H., Moise, A., Brown, S., Sargoytchev, S., Peterson, R.N., Shepherd, G.G., Lopez-Gonzalez, M.J., Lopez-Moreno, J.J., Rodrigo, R., 1997. SATI: a spectral airglow temperature imager. Advances in Space Research 19 (4), 677–680.

Xu, J., Liu, H.-L, Yuan, W., Smith, A.K., Roble, R.G., Mertens, C.J., Russell III, J.M., Mlynczak, M.G., 2007. Mesopause structure from thermosphere, ionosphere, mesosphere, energetics, and dynamics (TIMED)/sounding of the atmosphere using broadband emission radiometry (SABER) observations. Journal of Geophysical Research 112, D09102.

Yee, J.-H., Crowley, G., Roble, R.G., Skinner, W.R., Burrage, M.D., Hays, P.B., 1997. Global simulations and observations of O (^{1}S), O$_2$ ($^1\Sigma$) and OH mesospheric nightglow emissions. Journal of Geophysical Research 102 (A9), 19,949–19,968.

Younger, J.P., Reid, I.M., Vincent, R.A., Holdsworth, D.A., 2008. Modeling and observing the effect of aerosols on meteor radar measurements of the atmosphere. Geophysical Research Letters 35 (15), L15812.